CDF/PUB/JET/PUBLIC/577

Invited talk at 7th International Conference on "Physics in Collision", Tsukuba, Japan, August 25 - 27, 1987

Central Jets in the CDF experiment

The CDF collaboration *

Presented by Shinhong Kim

University of Tsukuba
Sakura, Niihiari, Ibaraki, Japan

1. Introduction

Proton-antiproton collisions, at center of mass energy of 1.8 TeV, were recorded in the CDF detector between March and May, 1987. The maximum instantaneous luminosity recorded was 1.5×10^{29} $cm^{-2}sec^{-1}$. The total integrated luminosity, for data logged on tape, was about 35 nb^{-1}.

At the energies of the CERN SPS $\bar{p}p$ collider ($\sqrt{s}$ = 546 and 630 GeV), hadronic jets were clearly identified by UA1 and UA2 collaborations [1]. Jet production properties have been investigated by measurements of the inclusive cross sections [2], of the two-jet angular distribution [3] and of three-jet cross section [4] and fragmentation properties of hadronic jets have also been studied [5].

In this paper, we show jets clearly seen at $\sqrt{s}$ = 1.8 TeV, the several properties of jets and the inclusive jet Et distribution measured at $\sqrt{s}$ = 1.8 TeV in the pseudorapidity range between -1 and 1 with the CDF detector. The slope of the inclusive jet Et distribution is compared with that obtained with ISAJET Monte Calro program .

2. CDF Detector

A cross sectional view of the CDF detector is shown in Fig.1. The CDF detector[6] consists of electromagnetic calorimeters, hadron calorimeters, muon

* The CDF collaboration is listed in Appendix 1.

chambers, tracking chambers and beam-beam counters. The total number of electronic channels for the entire system is about 70,000.

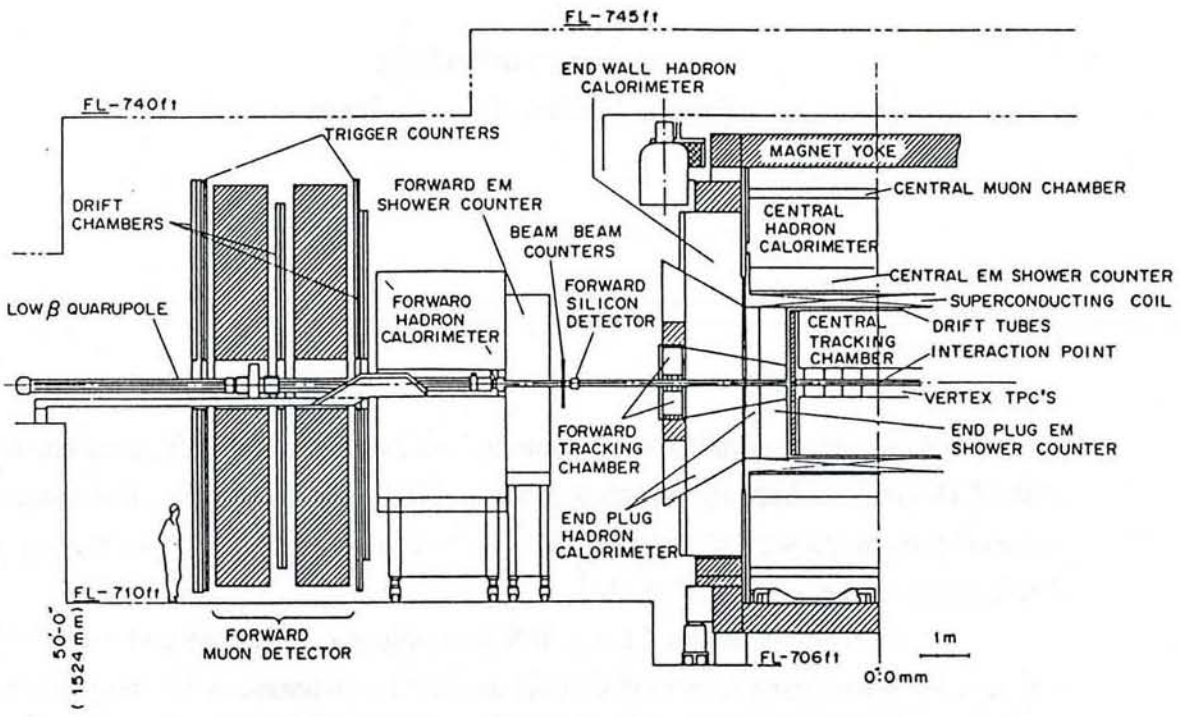

Fig.1 A cross sectional view of the CDF detector

The seven calorimeter systems[7] in the CDF detector include: the central EM calorimeter, the central hadron calorimeter, the endwall hadron calorimeter, the endplug EM calorimeter, the endplug hadron calorimeter and the forward EM and forward hadron calorimeters. All of the calorimeters are of the sampling type. The EM calorimeters use lead plates as the absorber; the hadron calorimeters use steel. In the central and endwall calorimeters the active medium is scintillator; the endplug and forward calorimeters use proportional tube chambers with cathode pad readout.

The CDF calorimetry has complete azimuthal coverage over the polar angles ranging from 2° to 178°, corresponding to pseudorapidity coverage from -4.2 to 4.2. The calorimeters are all subdivided into many cells, each having tower geometry where

each tower points to the center of the interaction region. The tower segmentation ($\Delta\eta$ x $\Delta\phi$) is 0.1 x 0.09 in the endplug and forward proportional chamber calorimeters, and 0.1 x 0.26 in the central and endwall scintillator calorimeters.

The energy resolution of each calorimeter system is shown in table 1; the energy resolution at Et = 50 GeV is approximately 2 % in EM calorimeters and 12 % in hadron calorimeters.

Table 1 Energy resolution of the CDF calorimetry

	Energy Resolution (σ/E)	
	E = 50 GeV	Et = 50 GeV
Central EM Calorimeter	2 %	2 %
Central Hadron Calorimeter	11 %	11 %
Endwall Hadron Calorimeter	14 %	12 %
Plug EM Calorimeter	3 %	2 %
Plug Hadron Calorimeter	20 %	12 %
Forward EM Calorimeter	4.5 %	2 %
Forward Hadron Calorimeter	23 %	14 %

The central calorimeter is comprised of 48 wedge modules, one of which is shown in Fig.2. Ten towers of the EM calorimeter are located at the inner surface. Lead plates, each 3.2 mm thick, are sandwiched between 31 layers of 5 mm thick polystyrene scintillator. A proportional tube chamber is imbedded in the stack at a depth of about 5 radiation lengths. The center of gravity of EM showers is determined in this chamber with an accuracy of 2 mm . Y7 wavelength shifters on the two sides of a tower collect light from the scintillator. Light guides carry the light to two phototubes per tower on

the back of the modules. There are eight hadron towers in each wedge module. Each tower has two phototubes arranged similarly to those in the EM towers.

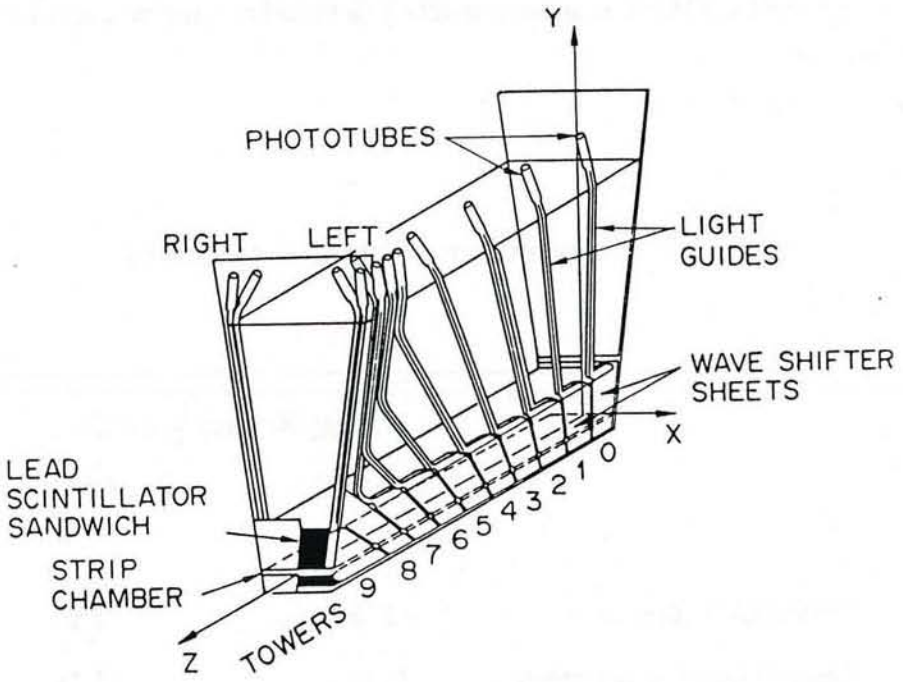

Fig.2 One of 48 wedge modules which compose the central calorimeter

3. Calibration of CDF central calorimeter

The CDF central EM calorimeter was calibrated in a test beam of 50 GeV electrons. This calibration has been maintained over time by means of individual Cs137 sources for each module. The ratio of the 50 GeV electron response to the response to a Cs137 source is assumed to be constant. Figure 3 shows the difference in the ratio of the response to the electron beam to that for the Cs137 source, for succesive calibration procedures separated in time by about 5 weeks, for four different modules. The 0.2% deviation in the mean value corresponds accurately to the current decrease expected from the disintegration of the Cs sources. These data indicate that the calibration is reproducible at the $\pm$ 0.7 % level.

The central hadron calorimeter was also calibrated in a test beam of 50 GeV pions. The pulse height distribution for 50 GeV pions that give minimum ionizing

pulses in the EM section is shown in Fig.4. A peak around 2 GeV is due to muon contamination in pion beam. The conversion coefficient from ADC counts to energy was obtained from this pion peak. The calibration reproducibility was tested in the same way as for the EM calorimeter. The percentage difference between corresponding pion peaks normalized by Cs137 source current of 7 recalibrated modules is plotted in Fig.5. Here the reproducibility is at the 1% level.

Fig. 3 Calibration reproducibility of the central EM calorimeter
Fig. 4 Pulse height distribution for 50 GeV poins of the central hadron calorimeter
Fig. 5 Calibration reproducibility of the central hadron calorimeter

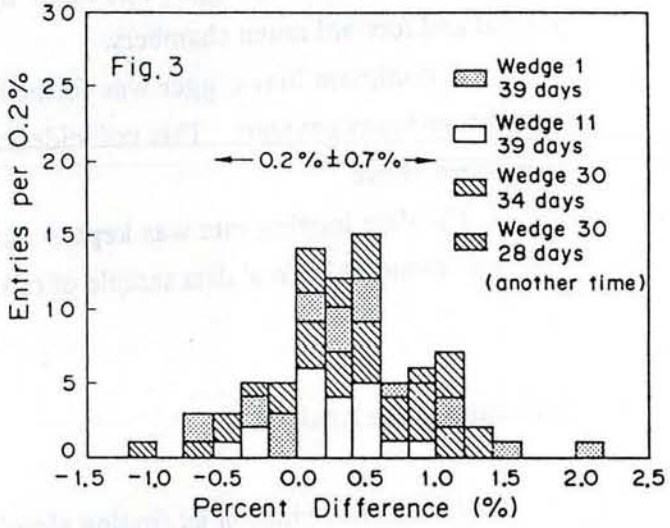

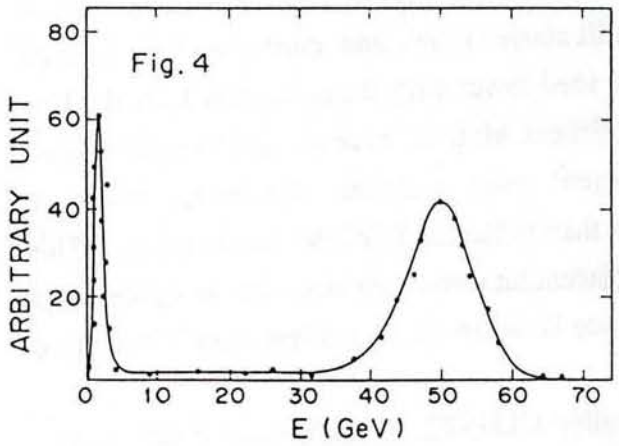

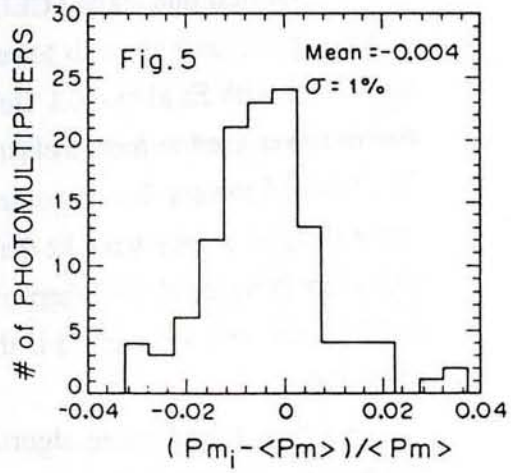

4. Data Acquisition

We took the data with several kinds of triggers simultaneously, with trigger threshold values that varied, depending on the luminosity:

A total Et trigger was made from the sum of the Et deposited in the central calorimeter. The threshold was set to 20, 30, 40 or 45 GeV depending on the luminosity. Another total Et trigger was made from the sum of Et deposited in either the plug EM calorimeters or the forward EM calorimeters. This threshold varied from 10 to 15 or 20 GeV.

An electron trigger was formed using the sum of Et deposited in the central EM calorimeter, selecting only those towers that had Et above 5 GeV. The total Et threshold was set to 15 GeV.

A high pt muon trigger was made by a tracking processor associated with the central and forward muon chambers.

A minimum bias trigger was formed from coincidences between the West and East beam-beam counters. This coincidence was also required for the three triggers mentioned above.

The data logging rate was kept to about 1 Hz and the number of jet events per tape was about 300. Total data sample of run amounted to about 500 tapes.

5. Results of the Analysis

We used two kinds of jet finding algorithms for performing the jet analysis:

The first one, called CLUST2, is based on nearest neighbor clustering. In the clustering, we pick as seeds towers with Et above 1 GeV and cluster with it adjoining hit towers with Et above 0.1 GeV. The seed tower with the maximum Et is the first parent tower used to form a cluster. Adjacent hit towers are merged into the cluster. The merged towers then become new parent towers and their adjacent hit towers are again merged if they have Et that is less than twice the Et of the parent tower. This procedure is repeated until there are no adjacent hit towers. Finally after all clustering is finished, clusters are merged if the distance between the two is less than 0.7 in η - ϕ coordinates.

Another jet finding algorithm, called CLUST3, is an Et-dependent window clustering. This algorithm is based on the hypothesis that the average momentum of particles transeverse to jet axis is independent of jet energy, in that case, the jet size in the η - ϕ plane is inversely proportional to the jet Et. In this algorithm, we start by picking up seed towers and hit towers in the same way as CLUST2. The cluster boundary radius is set to 12.0/Et (Et in GeV) and 0.6, whichever is smallest. After merging all of the hit towers within this boundary into a cluster, we recalculate Et sum and obtain new

cluster boundary radius with a new Et. This procedure is repeated until the fifth iteration or when the difference between the new and old Et is less than 2%. After clustering is finished, cluster merging is performed in the same way as in CLUST2.

In this analysis, we set the jet Et threshold to 10 GeV. The jet energy was defined to be the simple sum of the EM and hadronic energy. A typical two jet event in the CDF is shown in Fig.6. The jet characteristics obtained with the CLUST2 algorithm, such as jet Et, jet center of gravity, EM energy fraction and number of towers, are shown. In this event, the two jets have Et's of 83 and 75 GeV. The opening angle in ϕ between the two jets is 184 degrees, indicating that this event is a back-to-back 2 jet event. We also show the same event as it appears in the central tracking chamber. Many stiff tracks point to the two calorimeter clusters. From the tracking chamber, we can clearly recognize this as a clean two jet event.

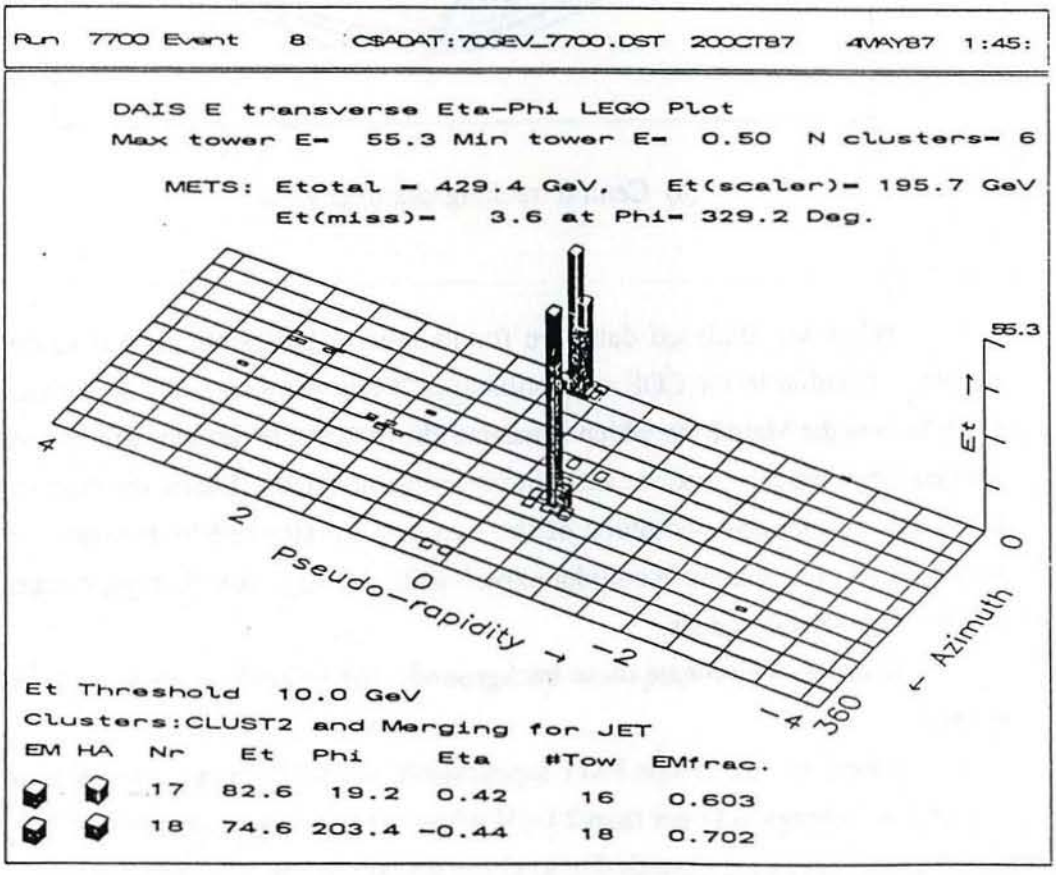

Fig.6 A typical two-jet event

(a) Calorimeter LEGO plot

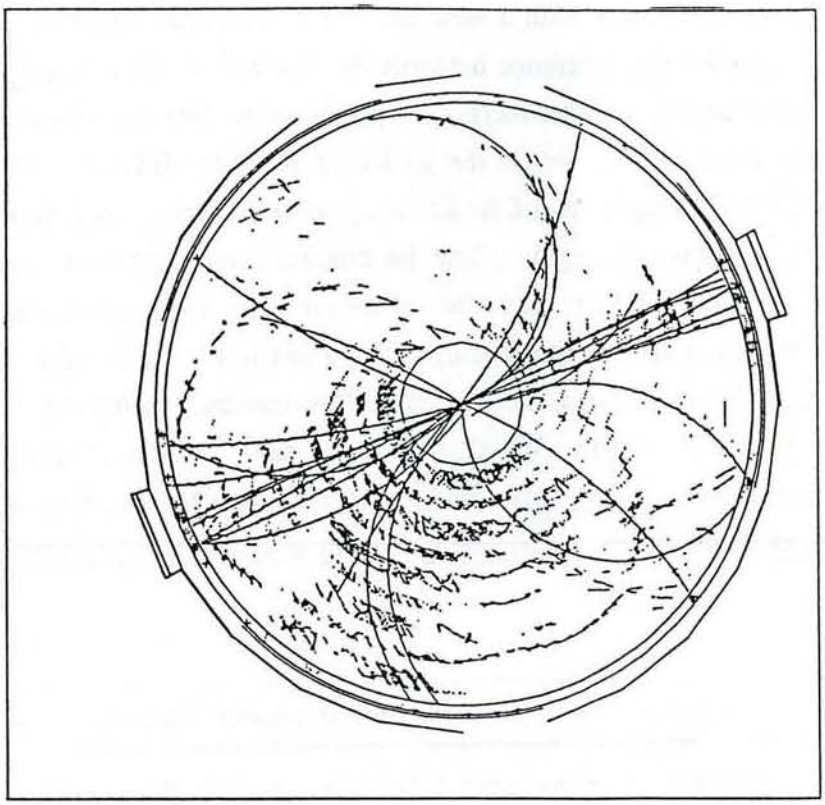

(b) Central tracking chamber view

When we analysed data, we found several backgrounds that cause fake jet events. Peculiar to the CDF environment is "Main Ring splash", background due to beam halo in the Main Ring which is located above the CDF detector and operates during data taking in order to produce antiprotons for the next fill. Phototube discharge results in signals in only one phototube of the two that are attached to a tower. The other backgrounds are common in collider experiments, namely: cosmic rays, electronic noise and beam gas backgrounds.

In order to eliminate these backgrounds, the following cuts were applied to jet events:

In the first cut, 'Single PMT suppression', we set the tower energy to zero if the higher PMT energy is larger than 2 GeV while the lower is smaller than 0.1 GeV. With this cut we reduce backgrounds due to single phototubes and electronic noise.

In the "TOF" cut, we make use of TDC information from the hadron calorimeter scintillators, rejecting those events that occur outside of a 35 nsec window inside of the 700 nsec event gate used for calorimeter signal readout. This cut reduces backgrounds

due to Main Ring splash, cosmic rays and beam-gas interactions by a factor of 20.

In the "EM energy fraction" cut, we eliminate hadron-rich jets with an EM energy fraction that is less than 0.1. This also suppresses backgrounds due to Main Ring splash, cosmic rays and beam-gas interactions.

Figure 7 shows the EM energy fraction in jets before and after the TOF cut. The peak around 0 becomes small after the cut; the mean value of EM fraction is about 0.6.

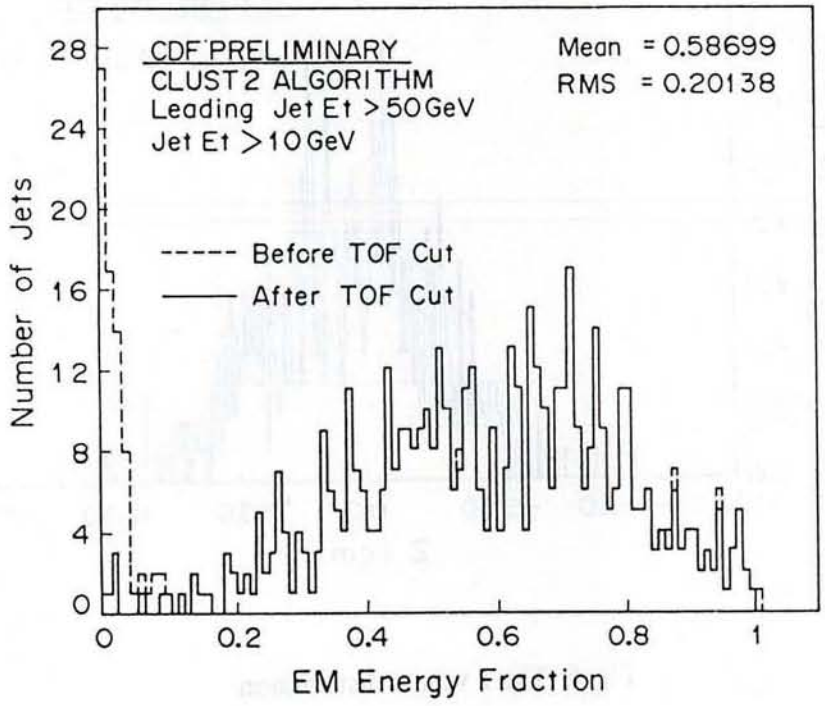

Fig. 7 Electromagnetic energy fraction in jets. Broken line and solid line indicate the distributions of the EM energy fraction in jets before and after TOF cut, respectively.

The following data samples were analysed for this talk: For the data with central total Et trigger thresholds of 20, 30, 40 and 45 GeV, we applied leading jet Et thresholds of 30, 40, 50 and 70 GeV, respectively. The integrated luminosities for the analysed data samples are .17, 1.5 , 11 and 22 nb^{-1} for leading jet Et threshold of 30, 40, 50 and 70 GeV; here the 50 GeV and 70 GeV data samples overlap.

In the analysis of each event, the z vertex was reconstructed using the information from the Vertex TPC and used for calculating the pseudorapidity for each

tower center. The z vertex distribution is shown in Fig.8. The r.m.s. spread of z vertex was 35 cm.

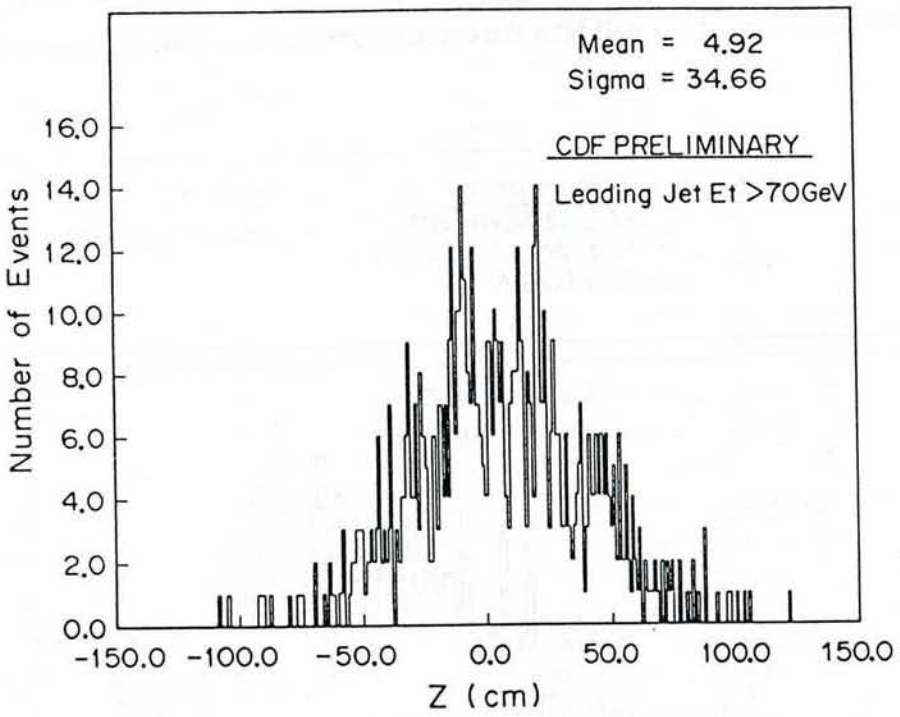

Fig. 8 The z vertex distribution

We discuss the following properties of jets: Jet azimuthal angle , ϕ, distribution, the angular correlation between jets, and the jet size. The distribution of azimuthal angles for the jets is expected to be uniform, in the absence of gain nonuniformity and acceptance bias. The jet azimuth distribution was fitted with a constant straight line with a chi-square per degree of freedom of 1.2, as shown in Fig. 9. This indicates that to within our current statistical precision, the calorimeter gains are uniform and the acceptance is unbiased.

The opening angle in ϕ between the leading jet and the second highest Et jet is shown in Fig.10. The mean value is very close to 180 degrees and the spread is narrow. The tendency for jets to be back-to-back is clear from this plot.

Jet sizes are studied using the following variables: σ_ϕ is a standard deviation width of a jet in azimuth weighted by Et; σ_η is the corresponding width in

pseudorapidity. A scatterplot of σ_ϕ versus σ_η is shown in Fig.11. Most of jets have the width smaller than 0.4 both in η and ϕ. A distribution for a one-dimensional jet-size parameter, D, defined as $D = \sqrt{(\sigma_\phi^2 + \sigma_\eta^2)}/2$, is shown in Fig.12; this plot indicates that the mean jet width is 0.19.

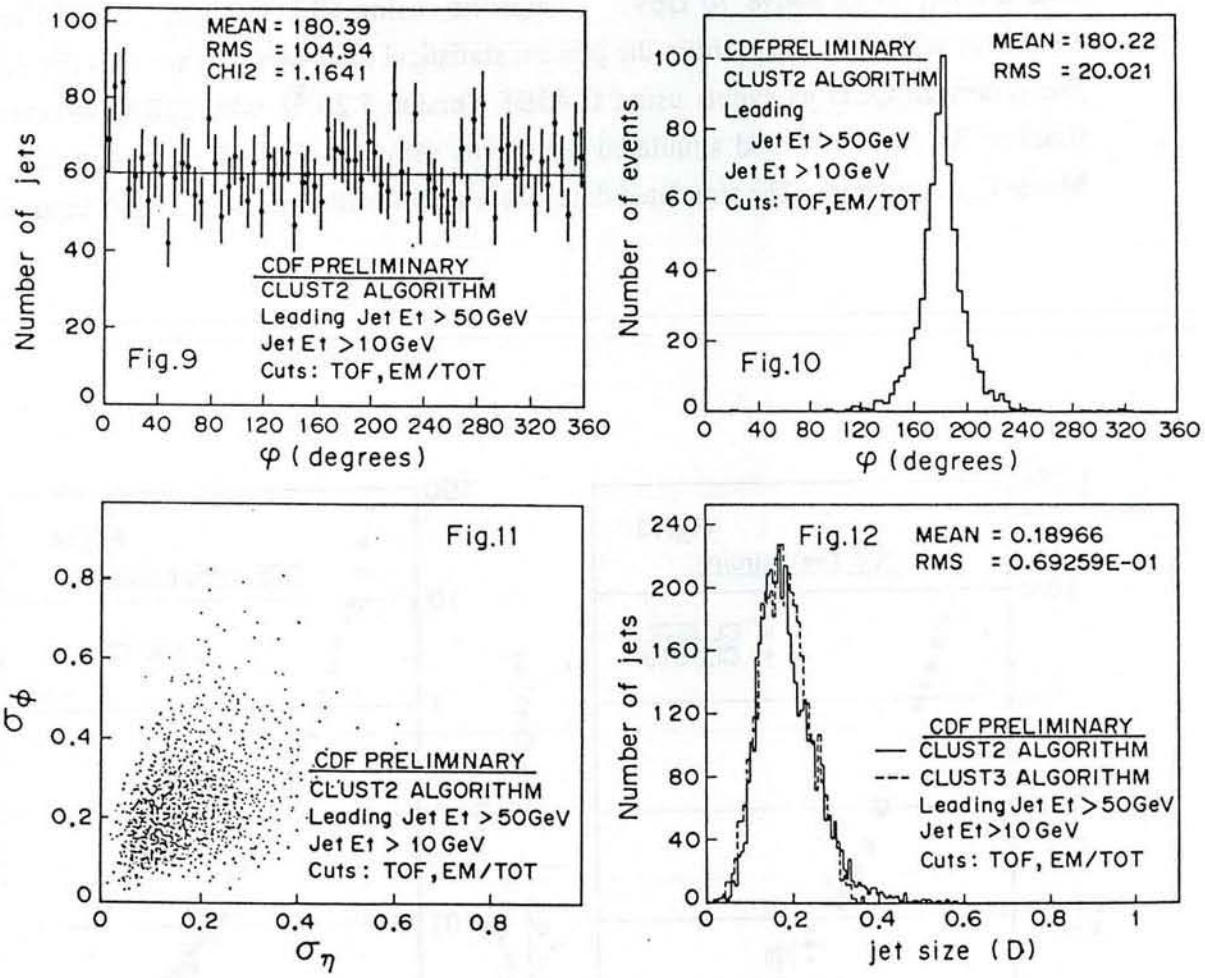

Fig. 9 The jet azimuth distribution. A fitted straight line is also shown in this figure.

Fig.10 The opening angle in ϕ between the leading jet and the second highest Et jet.

Fig.11 A scatter plot of the jet width in azimuth (σ_ϕ) versus the jet width in pseudo-rapidity (σ_η).

Fig.12 One dimensional jet width (D). A broken line and a solid line show the distribution of the jet width using CLUST3 and CLUST2, respectively.

The jet properties mentioned so far are very similar for the CLUST2 and CLUST3 clustering algorithms. Only the jet-size distribution showed a slight difference

between the two approaches.

We obtained inclusive jet Et distributions for the pseudorapidity range between -1 and 1. The event samples already mentioned were used, corresponding to integrated luminosity of 24 nb^{-1} (about two thirds of the total logged data sample). The data samples with leading jet Et above 30, 40 and 50 GeV are normalized to the data samples with leading jet Et above 70 GeV. Results using CLUST2 and CLUST3 are consistent with each other within the present statistical precision, as shown in Fig.13. We generated QCD jet events using ISAJET Version 5.20 [8] with EHLQ structure function Solution 1 [9] and simulated the events using the CDF detector simulation Monte Carlo program. The simulated data was analysed with the same analysis program

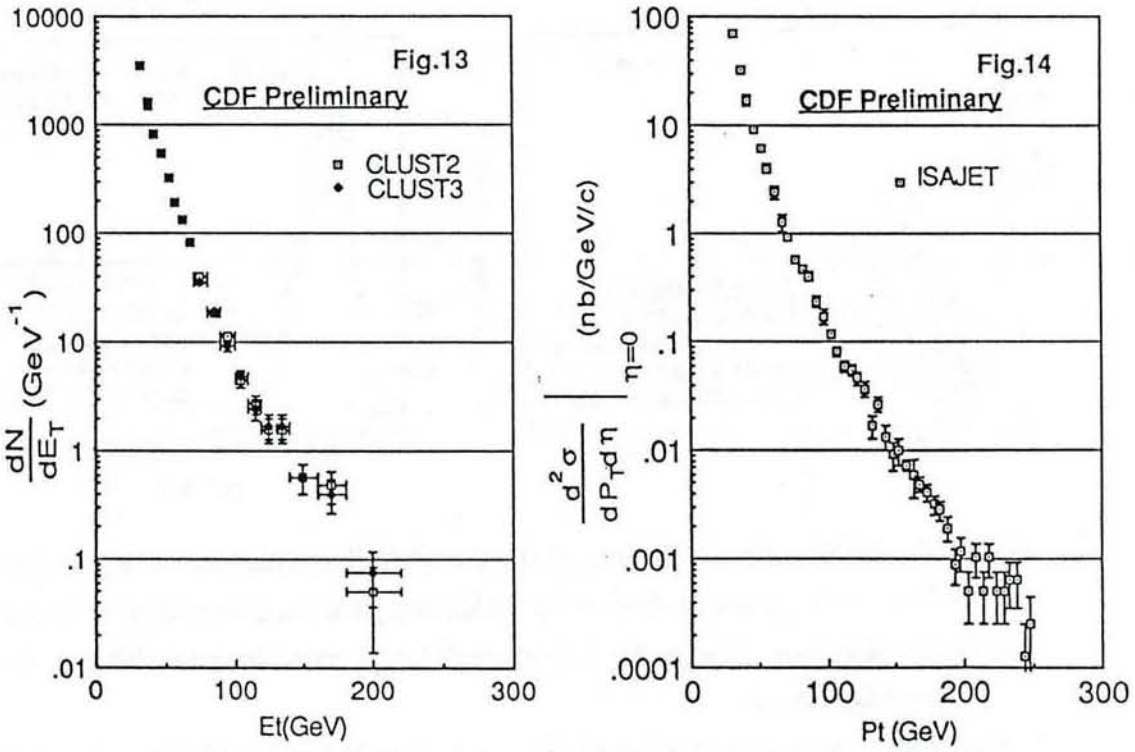

Fig. 13 Inclusive jet Et distributions for $-1 < \eta < 1$ using CLUST2 and CLUST3.

Fig. 14 Monte Carlo Et cross section with ISAJET and CDF simulation program.

as used in the analysis of the real data using CLUST2. The slope of the CDF Et distribution (Fig.13) is consistent with the slope of the Monte Carlo Et distribution, shown in Fig.14. This indicates that the detector simulation of the acceptance and calorimeter response is reasonable and that the measured slope of the jet Et distribution is consistent with QCD.

A number of corrections to the energy distribution still need to be made. These include corrections for detector performance such as for EM-hadron energy sharing, low energy response and lateral(crack) and longitudinal shower leakage. When we compare our results with theoretical QCD calculations at the parton level, we will need to correct for the differences between the jet energy and the final state parton energy.

6. Summary

Jet events are clearly observed in proton-antiproton collisions at a cms energy of 1.8 TeV. Back-to-back jets are clearly seen. The mean jet size is 0.2 in a standard deviation in the η - ϕ plane using the CDF jet finding algorithms, CLUST2 and CLUST3. Inclusive Jet Et distributions, formed using both jet finding algorithms are consistent with each other. It also has the same slope as predicted by the ISAJET Version 5.20 event generator and the CDF detector simulation program.

References

[1] Banner, M. et.al. (UA2) Phys. Lett. 118B, 203 (1982).
Arnison, G. et.al. (UA1) Phys. Lett. 123B, 115 (1983).

[2] Arnison, G. et.al. (UA1) Phys. Lett. 132B, 214 (1983).
Arnison, G. et.al. (UA1) Phys. Lett. 172B, 461 (1986).
Bagnaia, P. et.al. (UA2) Phys. Lett. 138B, 430 (1984).
Bagnaia, P. et.al. (UA2) Phys. Lett. 160B, 349 (1985).

[3] Arnison, G. et.al. (UA1) Phys. Lett. 136B, 294 (1984).
Arnison, G. et.al. (UA1) Phys. Lett. 177B, 244 (1986).
Bagnaia, P. et.al. (UA2) Phys. Lett. 144B, 283 (1984).

[4] Banner, M. et.al. (UA2) Z.Phys. C-Particles and Fields 20, 117 (1983).
Appel, J.A. et.al. (UA2) Z.Phys. C-Particles and Fields 30, 341 (1986).
Arnison, G. et.al. (UA1) Phys. Lett. 158B, 494 (1985).

[5] Arnison, G. et.al. (UA1) Phys. Lett. 132B, 223 (1983).
Arnison, G. et.al. (UA1) Phys. Lett. 147B, 222 (1984).
Bagnaia, P. et.al. (UA2) Phys. Lett. 144B, 291 (1984).
[6] CDF design report internal CDF report No.111 (1981) unpublished;
Jensen, H.B. IEEE Trans. Nucl. Sc. NS-33 No.1, 40 (1986).
[7] Jensen, H.B. Fermilab - Conf - 87/62 (1987).
[8] Paige, F.E. and Protopopescu, S.D. Proceedings of the UCLA Workshop on SSC Physics 213 (1986).
[9] Eichten, E., Hinchliffe,I., Lane, K. and Quigg, C. Rev. Mod. Phys. 56, 579 (1984).

Appendix 1: CDF Collaboration

F.Abe[p], D.Amidei[c], G.Apollinari[k], G.Ascoli[g], M.Atac[d], P.Auchincloss[n], A.R.Baden[f], A.Barbaro-Galtieri[l], V.Barnes[l], E.Barsotti[d], F.Bedeschi[k], S.Belforte[m], G.Bellettini[k], J.Bellinger[q], J.Bensinger[b], A.Beretvas[n], P.Berge[d], S.Bertolucci[e], S.Bhadra[g], M.Binkley[d], R.Blair[a], C.Blocker[b], J. Bofill[d], A.W.Booth[d], G.Brandenburg[f], A.Brenner[d], D.Brown[f], A.Byon[l], K.L.Byrum[q], M.Campbell[c], R.Carey[f], W.Carithers[l], D.Carlsmith[q], J.T.Carroll[d], R.Cashmore[1], F.Cervelli[k], K.Chadwick[l], T.Chapin[m], G.Chiarelli[m], W.Chinowsky[l], S.Cihangir[o], D.Cline[q], T.Collins[d], D.Connor[j], M.Contreras[b], J.Cooper[d], M.Cordelli[e], M.Curatolo[e], C.Day[d], R.DelFabbro[k], M.Dell'Orso[k], L.DeMortier[b], T.Devlin[n], D.DiBitonto[o], R.Diebold[a], F.Dittus[d], A.DiVirgilio[l], R.Downing[g], G.Drake[d], T.Droege[d], M.Eaton[f], J.E.Elias[d], R.Ely[l], S.Errede[g], B.Esposito[e], A.Feldman[f], B.Flaugher[n], E.Focardi[k], G.W.Foster[d], M.Franklin[g], J.Freeman[d], H.Frisch[c], Y.Fukui[h], I.Gaines[d], A.Garfinkel[l], P.Giannetti[2], N.Giokaris[m], P.Giromini[e], L.Gladney[j], M.Gold[l], K.Goulianos[m], J.Grimson[d], C.Grosso-Pilcher[c], C.Haber[l], S.Hahn[j], R.Handler[q], R.M.Harris[l], J.Hauser[c], Y.Hayashide[p], T.Hessing[o], R.Hollebeek[j], L.Holloway[g], P.Hu[n], B.Hubbard[l], P.Hurst[g], J.Huth[d], M.Ito[p], J.Jaske[q], H.Jensen[d], U.Joshi[n], R.W.Kadel[d], T.Kamon[o], S.Kanda[p], I.Karliner[g], H.Kautzky[d], K.Kazlauskis[n], E.Kearns[f], R.Kephart[d], P.Kesten[b], H.Keutelian[g], Y.Kikuchi[p], S.Kim[p], L.Kirsch[b], S.Kobayashi[3], K.Kondo[p], W.Krishuk[f], U.Kruse[g], S.Kuhlmann[l], A.Laasanen[l], W.Li[a], T.Liss[c], N.Lockyer[j], F.Marchetto[o], R.Markeloff[q], L.A.Markosky[q], M.Masuzawa[p], P.McIntyre[o], A.Menzione[k], T.Meyer[o], S.Mikamo[h], M.Miller[j], T.Mimashi[p], S.Miscetti[e], M.Mishina[h], S.Miyashita[p], H.Miyata[p], N.Mondal[q], S.Mori[p], Y.Morita[p], A.Mukherjee[d], A.Murakami[3], Y.Muraki[4], C.Nelson[d], C.Newman-Holmes[d], J.S.T.Ng[f], L.Nodulman[a], J.O'Meara[d], G.Ott[q], T.Ozaki[p], S.Palanque[d], R.Paoletti[k], A.Para[d], J.Patrick[d], R.Perchonok[d], T.J.Phillips[f], H.Piekarz[b], R.Plunkett[m], L.Pondrom[q], J.Proudfoot[a], G.Punzi[k], D.Quarrie[d], K.Ragan[j], G.Redlinger[c], R.Rezmer[a], J.Rhoades[q], L.Ristori[k], T.Rohaly[j], A.Roodman[c], H.Sanders[c], A.Sansoni[e], R.Sard[g], V.Scarpine[g], P.Schlabach[g], E.E.Schmidt[d], P.Schoessow[a], M.Schub[l], R.Schwitters[f], A.Scribano[k], S.Segler[d], M.Sekiguchi[p], P.Sestini[k], M.Shapiro[f], M.Sheaff[q], M.Shibata[p], M.Shochet[c], J.Siegrist[l], V.Simaitis[g], J.Simmons[l], P.Sinervo[j], M.Sivertz[5], J.Skarha[q], D.A.Smith[g], R.Snider[c], L.Spencer[b], R.St.Denis[f], A.Stefanini[k], Y.Takaiwa[p], K.Takikawa[p], S.Tarem[b], D.Theriot[d], J.Ting[c], A.Tollestrup[d], G.Tonelli[k], W.Trischuk[f], Y.Tsay[c], K.Turner[d], F.Ukegawa[p], D.Underwood[a], C.vanIngen[d], R.VanBerg[j], R.Vidal[d], R.G.Wagner[a], R.L.Wagner[d], J.Walsh[j], T.Watts[n], R.Webb[o], T.Westhusing[g], S.White[m], V.White[d], A.Wicklund[a], H.H.Williams[j], T.Winch[q], R.Yamada[d], T.Yamanouchi[d], A.Yamashita[p], K.Yasuoka[p], G.P.Yeh[d], J.Yoh[d], F.Zetti[k]

Argonne National Laboratory[a] - Brandeis University[b] - University of Chicago[c] - Fermi National Accelerator Laboratory[d] - INFN,Frascati,Italy[e] - Harvard University[f] - University of Illinois[g] - KEK, Japan[h] - Lawrence Berkeley Laboratory[l] - University of Pennsylvania[j] - INFN,University of Pisa,Italy[k] - Purdue University[l] - Rockefeller University[m] - Rutgers University[n] - Texas A&M University[o] - University of Tsukuba, Japan[p] - University of Wisconsin[q] Collaboration

[1]Visitor from University of Oxford, England.
[2]Visitor from INFN Trieste, Italy.
[3]Visitor from Saga University, Japan.
[4]Visitor from ICRR, Tokyo University, Japan.
[5]Visitor from Haverford College, Haverford, PA.